ARCHIVES
of
FOUNDRY ENGINEERING

ISSN (2299-2944)
Volume 2026
Issue 3/2026

45 – 53

10.24425/afe.2026.158017

6/3

Published quarterly as the organ of the Foundry Commission of the Polish Academy of Sciences

# Effect of Fuel Type on Flow-Thermal Field Evolution and Preheating Performance of Scrap in Molten Iron Ladle

**Yi ming Fu, Guang qiang Liu *, Lan yue Xu**
University of Science and Technology Liaoning, School of Civil Engineering, China
* Corresponding author: E-mail address: lgqiang0305@sina.com

Received 24.05.26; accepted in revised form 24.06.26; available online 31.08.2026

## Abstract

Against global carbon neutrality targets, the carbon-intensive steel industry bears severe decarbonization stress, wherein advanced low-carbon smelting technologies dominate its green transition. Scrap preheating boosts scrap ratio and cuts steelmaking carbon emissions; optimized fuel-scrap matching and fuel grading by scrap type significantly improve thermal efficiency and reduce preheating energy demand. This work establishes a 3D numerical model for randomly stacked scrap within a 100-t hot metal ladle to compare natural gas, coke oven gas and converter gas regarding flow field, flame structure, thermal distribution, scrap heating performance and energy efficiency under equal total heat input. Numerical simulations with the k-ε turbulence, EDC combustion and P-1 radiation models are performed to couple flow, heat transfer and combustion. Fuel composition strongly governs flame morphology and thermal behaviors. Natural gas and converter gas form intact, stiff flames, while coke oven gas produces discontinuous unstable flames. Flow intensity decreases in the sequence converter gas, coke oven gas and natural gas, and high-speed turbulent fluctuation of converter gas facilitates heat diffusion. Under the same heating duration, the average surface temperatures of scrap are 695 K, 782 K and 411 K for natural gas, converter gas and coke oven gas, respectively. Converter gas achieves the highest preheating efficiency of 11.2 %, followed by natural gas (5.9 %), and coke oven gas is the lowest (2.4 %) due to its low calorific value. Moreover, fuel-scrap matching characteristics reveal that natural gas is suitable for light and thin scrap to avoid overheating, while converter gas is more favorable for medium and heavy scrap with improved heat penetration. This work reveals the influence mechanism of gas type on ladle scrap preheating and provides theoretical support for fuel selection and process optimization in high-efficiency and low-carbon scrap preheating applications.

**Keywords:** Scrap preheating, Fuel type, Flow-thermal field, Flame morphology, Preheating efficiency

## 1. Introduction

Scrap, as a renewable resource, plays a vital role in reducing iron ore consumption, energy demand and pollutant emissions [1, 2]. With increasing global pressure on carbon emission reduction, raising the scrap ratio has become a key pathway for steel enterprises to lower costs and improve environmental performance [3,4]. However, due to the limited surplus heat of molten steel, the scrap ratio in conventional converters is usually below 20%. Scrap preheating, which heats scrap to a certain temperature before charging, can effectively supplement the heat required in the smelting process and has become an essential technique for high-scrap-ratio steelmaking [5]. Nevertheless, traditional preheating methods suffer from low thermal efficiency and insufficient waste heat recovery [6], and stand-alone preheating equipment increases overall energy consumption [7, 8].

The scrap preheating process involves complex multi-physics phenomena, including turbulent combustion, gas-solid heat

© The Author(s) 2026. Open Access. This article is licensed under a Creative Commons Attribution 4.0 International License (http://creativecommons.org/licenses/by/4.0/), which permits use, sharing, adaptation, distribution and reproduction in any medium or format, as long as you give appropriate credit to the original author(s) and the source, provide a link to the Creative Commons licence, and indicate if changes were made.

transfer and thermal radiation. Many researchers have carried out numerical and experimental studies on this topic. Fan et al. [9] compared the preheating performance of a vertical three-stage furnace and a horizontal tunnel furnace, finding that the vertical furnace achieved a scrap heat absorption efficiency of 63% under the same fuel heat input, significantly higher than 35% for the horizontal furnace. Zhang et al. [10] developed a 3D numerical model of a 90 t hot metal ladle and quantitatively analyzed the effects of ambient temperature, wind speed, slag thickness and ladle cover thickness on the temperature drop of hot metal. Vodička et al. [11] studied the melting behavior of scrap in a ladle with bottom argon blowing using a multi-physics model, showing that increasing the specific surface area and initial temperature of scrap significantly accelerates the melting rate. Poraj et al. [12] compared a DC plasma torch and natural gas heating for a steelmaking ladle, demonstrating that plasma heating achieved a higher ladle bottom temperature (983-1402 °C) than natural gas (874 °C).

Aiming at the problems of low efficiency and single fuel selection of traditional preheating methods, this paper carries out comparative research on multiple fuels, so as to solve the practical deficiencies in on-site production.

Although previous studies have advanced the understanding of scrap preheating, most of them focused on a single fuel or did not systematically compare different fuels under identical total heat input[13, 14]. To tackle the low efficiency and monotonous fuel selection of traditional preheating processes, this study performs a comparative analysis of diverse fuels for eliminating practical drawbacks in actual production. A three-dimensional numerical model of randomly stacked scrap in a 100 t hot metal ladle was established. Natural gas, coke oven gas and converter gas are selected as typical industrial fuels. Under the same total heat input, the flow field, flame morphology, temperature field and scrap temperature evolution are systematically compared. This work aims to reveal the influence mechanism of fuel type on scrap preheating and to provide theoretical guidance for fuel selection and process optimization.

# 2. Mathematical and physical modelling of scrap preheating

## 2.1. Basic governing equations and mathematical models

The scrap preheating process involves complex momentum transfer, heat transfer and mass transfer phenomena, all following fundamental conservation laws. This study solves the continuity equation, momentum equations, energy equation and k-ε equations to characterize the flow, heat transfer and combustion characteristics. The main governing equations are as follows [15, 16]:

Continuity equation.

$$\frac{\partial \rho}{\partial t}+\frac{\partial(\rho u)}{\partial x}+\frac{\partial(\rho v)}{\partial y}+\frac{\partial(\rho w)}{\partial z}=0 \tag{1}$$

Momentum conservation equation [14]:

.

$$\frac{\partial}{\partial t}(\rho u_i)+\frac{\partial}{\partial x_j}(\rho u_i u_j)=-\frac{\partial p}{\partial x_i}+\frac{\partial \tau_{ij}}{\partial x_j}+\rho g_i+S_i \tag{2}$$

Energy conservation equation [15]:

$$\frac{\partial}{\partial t}(\rho h)+\frac{\partial}{\partial x_i}(\rho u_i h)=\frac{\partial}{\partial x_i}\left(k\frac{\partial T}{\partial x_i}-\sum_j h_j J_{j,i}\right)+\frac{\partial p}{\partial t}+u_i\frac{\partial p}{\partial x_i}+\tau_{ij}\frac{\partial u_i}{\partial x_j}+S_h \tag{3}$$

In the formula (1)-(3): ρ is the density; t is time; u, v, and w are the velocity components in the x, y, and z directions, respectively. $\tau_{ij}$ is the viscous stress tensor; $S_i$ is the source term in the momentum equation. $h$ represents the total enthalpy; $k$ denotes the thermal conductivity; $T$ is the temperature; $J_{j,i}$ is the diffusion flux of component $j$; $u_i\partial p/\partial x_i$ denotes the convective pressure term; $\tau_{ij}\partial u_i/\partial x_j$ represents the viscous stress term (with $\tau_{ij}$ being the viscous stress tensor); $\partial u_i/\partial x_j$ is the velocity gradient; $u_i$ is the velocity component in the i-direction; $S_h$ is the energy source term; and $\partial p/\partial t$ is the time derivative of pressure.

The turbulence model is the k-ε model [17]. The transport equations for turbulent kinetic energy k and its dissipation rate ε are:

k equation:

$$\frac{\partial}{\partial t}(\rho k)+\frac{\partial}{\partial x_j}(\rho k u_i)=\frac{\partial}{\partial x_j}\left[\left(\eta+\frac{\eta_t}{\sigma_k}\right)\frac{\partial k}{\partial x_j}\right]+\eta_t\frac{\partial u_i}{\partial x_j}\left(\frac{\partial u_i}{\partial x_j}+\frac{\partial u_j}{\partial x_i}\right)-\rho\varepsilon \tag{4}$$

ε equation:

$$\frac{\partial}{\partial x_j}(\rho\varepsilon)+\frac{\partial(\rho u_i \varepsilon)}{\partial x_i}=\frac{\partial}{\partial x_i}\left[\left(\eta+\frac{\eta_t}{\sigma_\varepsilon}\right)\frac{\partial \varepsilon}{\partial x_i}\right]+c_1\rho S\varepsilon-c_2\rho\frac{\varepsilon^2}{k+\sqrt{\nu\varepsilon}} \tag{5}$$

In the formula (4)-(5): $k$ stands for turbulent kinetic energy; $\varepsilon$ represents the dissipation rate of $k$; $Sk$ and $S\varepsilon$ are the source terms of k and ε; $u_i$ denotes the mean velocity; $C_{1\varepsilon}$ and $C_{2\varepsilon}$ are empirical constants; typically, $C_{1\varepsilon}$=1.44, $C_{2\varepsilon}$=1.92, $C_\eta$=0.09, $\sigma_\varepsilon$=1.2, $\sigma_k$=1.0 [18].

The combustion model adopts the Eddy Dissipation Concept (EDC) model. The net reaction rate of species i is given by [19]:

$$\omega_i=\frac{\rho\xi^*}{\tau^*(1-\xi^*\gamma^*)}(Y_i^*-Y_i) \tag{6}$$

In the formula: $\omega_i$ represents the mass generation rate of substance $i$; $\xi^*$ denotes the mixing fraction; $\tau^*$ indicates the mixing time scale; $\gamma^*$ is the reaction volume fraction; $Y_i^*$ refers to the mass fraction of species after the reaction; and $Y_i$ represents the mass fraction of species before the reaction.

The P-1 radiation model is used for radiation heat transfer:

$$\frac{dI(\vec{r},\vec{s})}{dx}+(a+\sigma_s)I(\vec{r},\vec{s})=an^2\frac{\sigma T^4}{\pi}+\frac{\sigma_s}{4\pi}\int_0^{4\pi}I(\vec{r},\vec{s}')\Phi(\vec{s},\vec{s}')d\Omega' \tag{7}$$

In the formula: $I$ represents the radiation intensity; $r$ is the position vector; $s$ is the direction vector; $a$ is the absorption coefficient; $\sigma_s$ is the scattering coefficient; $n$ is the refractive index; $\sigma$ is the Stefan-Boltzmann constant; $s'$ denotes the scattering direction; $s$ is the optical path length; $\Phi$ is the phase function; $\Omega'$ is the spatial solid angle.

## 2.2. Model assumptions

1) No internal heat sources.
2) Only gas-solid convective and radiative heat transfer is considered within the scrap bed; other heat transfer modes are ignored.
3) Gases are ideal gases, and the heat transfer process between scrap and high-temperature flue gas is assumed to be transient.
4) Scrap melting collapse is not considered (no displacement occurs).

## 2.3. Physical model and mesh

The 100 t hot metal ladle is modelled using SpaceClaim 2023. The ladle has an upper diameter of 2400 mm, a lower diameter of 2100 mm and a total height of 3200 mm. The system is equipped with seven nozzles: the central nozzle is reserved for fuel feeding, and the six surrounding nozzles deliver combustion air. Flue gas is discharged through a 100 mm gap formed between the ladle cover and ladle rim, with all burner inlets having a uniform diameter of 80 mm.

The ladle consists of three layers from outside to inside: the steel shell, the permanent layer and the working layer. The bottom material is the same as the wall but with different thicknesses. Specific dimensions are given in Table 1.

The scrap dimensions inside the ladle refer to statistical data from actual steel plant production. A random stacking method is used to generate the three-dimensional geometry of the scrap bed. According to the plant charging method, from bottom to top: light-gauge scrap, light scrap, medium-heavy scrap and bales. Table 2 classifies four types of steel scrap with clear specifications on maximum dimensions in millimetres and typical shapes. Light-gauge scrap is limited to 300×300 mm in size and under 2 mm thick, appearing as thin metal plates. Light scrap allows a larger 400×400 mm overall size with thickness over 2 mm, consisting of metal strips and flat plates. Medium-heavy scrap features a maximum dimension of 600×400 mm and a thickness above 6 mm, covering structural forms such as I-beams, cylindrical metal pieces and spherical scraps. Bales refer to compacted scrap cubes no larger than 200×200 mm. The categorization relies on two key indicators: outer size and material thickness, paired with representative physical shapes to distinguish light, medium-heavy and compressed scrap grades. This standardized classification facilitates scrap sorting, transportation and smelting by clearly differentiating thin lightweight sheets, thicker metal profiles, heavy structural steel pieces and dense compressed bales for metal recycling facilities. Based on experimental and literature data, the porosity of the scrap bed is set to 0.45 [13].

Meshing is performed using Fluent Meshing. The computational domain mesh model is shown in Figure 1b. The model uses an unstructured mesh with approximately 1.41 million cells. The global average orthogonal quality is >0.9, meeting Fluent convergence requirements.

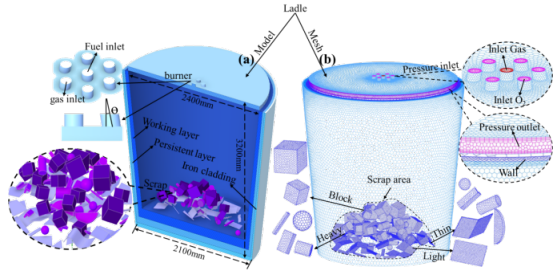



Fig.1 Schematic diagram of the molten iron ladle structure: (a) longitudinal section of the molten iron ladle; (b) mesh of the molten iron ladle

Table 1
Materials and dimensions of ladle layers

| Layer | Working layer | Permanent layer | Ladle shell |
|---|---|---|---|
| Material | Low-aluminum silicon carbide carbon brick | Fireclay brick | Q345 carbon steel |
| density, g/cm$^3$ | 2.6 | 1.8 | 7.85 |
| thermal conductivity, /W/m K | 12 | 1.2 | 45 |
| specific heat capacity, kJ/(kg·K) | 0.85 | 0.92 | 0.46 |
| Ladle sidewall thickness, mm | 135 | 85 | 36 |
| Ladle bottom thickness, mm | 180 | 130 | 75 |

Table 2
Scrap classification for simulation

| Type | Dimensions (mm) | Shape |
|---|---|---|
| Light-gauge scrap | ≤300×300, thickness <2 | Thin plate |
| Light scrap | ≤400×400, thickness >2 | Strip, plate |
| Medium-heavy scrap | ≤600×400, thickness >6 | I-beam, cylindrical, spherical |
| Bales | ≤200×200 | Cube |

## 2.4. Boundary conditions and fuel types

The finite difference method is used to discretize and solve the governing equations. The velocity-pressure coupling is handled using the improved SIMPLEC algorithm. The under-relaxation factor is set to 1.0 according to the characteristics of the model grid, flow field state and repeated debugging of numerical calculation. This parameter configuration can ensure the stability and convergence of the solving process. The supplementary content perfects the description of numerical solution settings. The number of time steps is determined based on the actual scrap preheating duration, with a maximum of 20 iterations per time step. Spatial discretization uses the second-order upwind scheme. Convergence

criteria are: residuals for the energy equation less than $10^{-6}$, and residuals for other governing equations less than $10^{-3}$.[17]

The relevant boundary and initial conditions are as follows: (1) Fuel inlet and combustion air inlet are both velocity inlets; initial scrap temperature is 300 K. (2) Flue gas outlet and the annular gap at the ladle cover are pressure outlets, with outlet pressure equal to ambient atmospheric pressure. (3) Initial ambient temperature is 300 K, initial pressure is 101.325 kPa.

Three fuels are studied: natural gas, coke oven gas and converter gas. Their compositions are given in Table 3. Under the same total heat input, the calculated flow rates are: natural gas 300 m³/h, coke oven gas 810 m³/h, converter gas 1320 m³/h.

Table 3
Volume fraction of fuel components (%)

| Component | Natural gas | Coke oven gas | Converter gas |
|---|---|---|---|
| CO | 0.3 | 9.0 | 60.2 |
| $CO_2$ | 1.0 | 2.3 | 14.6 |
| $H_2$ | 0.7 | 53.6 | 1.0 |
| $N_2$ | 4.0 | 16.4 | 18.0 |
| $O_2$ | 0.2 | 3.0 | 0.2 |
| $H_2O$ | – | – | 5.7 |
| $CH_4$ | 93.8 | 15.7 | – |
| lower calorific value MJ/Nm³ | 35.6 | 17.4 | 7.0 |

## 2.5. Model validation

To validate the accuracy and reliability of the established numerical model, simulation results are compared with industrial measurements from the literature [16] at five uniformly arranged monitoring points (A to E) on the ladle inner wall. The industrial measurement data were acquired via high-precision contact sensors mounted tightly on the ladle inner wall under actual production operating conditions, with continuous data sampling adopted to eliminate instantaneous measurement fluctuations and ensure the authenticity and representativeness of the original data. Prior to comparison, raw experimental data were preprocessed by filtering out abnormal noise points and calibrating instrument systematic errors, while the simulation data were extracted at the exact spatial coordinates corresponding to the field monitoring points to guarantee the consistency of comparison conditions. Furthermore, the model prediction error was effectively optimized by refining the mesh division near the ladle wall and correcting the boundary condition parameters.

Figure 2 shows the comparison between simulated and measured values. The overall trends are consistent, with only local deviations. The relative errors at points A and D are 6.1% and 2.2%, respectively, with a maximum temperature difference of 81 K. For the remaining monitoring points, the difference between simulated and measured temperatures is about 40 K, with relative errors around 2%. The comparison confirms that the model has high computational accuracy and can well reflect the actual temperature distribution during scrap preheating.

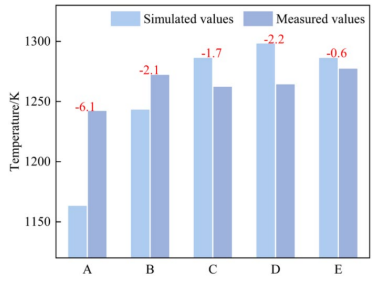


Fig. 2. Comparison of simulated and measured temperatures for scrap preheating

# 3. Analysis of preheating effects with different fuel types

## 3.1. Effect of fuel type on flow field inside the ladle

Figure 3 shows the flow field distribution in the Z=0 m vertical plane and Y=2 m horizontal plane for different fuels. Due to the different calorific values, under the same heating value, natural gas (Figure 3a) exhibits a relatively low velocity range (only 2-16 m/s), converter gas (Figure 3b) has the highest velocity (5-65 m/s), and coke oven gas (Figure 3c) is intermediate, with velocities ranging from 5-40 m/s. At the Z=0 m section, the velocity is highest in the central region of the fuel. The randomly stacked scrap will block and divert the fuel jet, change the propagation path of airflow, and further affect the distribution of velocity field and vortex structure. Different stacking states will lead to differences in jet disturbance range.

Different fuels exhibit distinct differences in the velocity distribution characteristics of combustion flow fields due to variations in physical parameters such as components, calorific values and injection flow velocities. Natural gas features a single component and high calorific value, with favorable jet flow stability and a relatively regular flow field structure. Its velocity gradient and vortex structure are symmetrically distributed with a wide influence range (dashed area in Fig. 3a). Converter gas presents a higher peak flow velocity and a drastically turbulent flow field, accompanied by an increased number of vortices with complex morphologies (dashed area in Fig. 3b). This indicates intense flow disturbance in and around the jet center, which is conducive to enhancing heat transfer and mass mixing. The flow field characteristics of coke oven gas fall between the above two fuels, with a more compact vortex structure. Its flow velocity and turbulence intensity are lower than those of converter gas but higher than those of natural gas, which directly reflects the regulatory effect of fuel physical properties on turbulent flow structures (dashed area in Fig. 3c). As illustrated in Fig. 4, the velocity distribution of natural gas and coke oven gas is relatively uniform, with a smaller high-velocity region and lower velocity peak compared with converter gas, leading to an overall homogeneous flow field. Affected by its high flow velocity, converter gas generates severe flow disturbance in the central and surrounding areas, thereby facilitating efficient heat transfer.

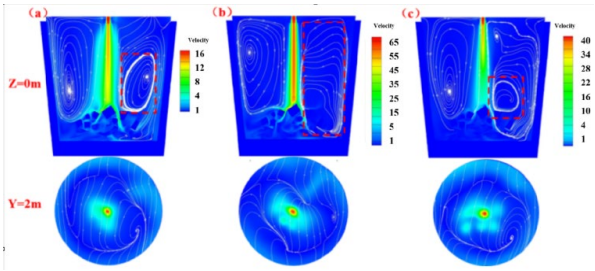



Fig. 3. Flow field distribution inside the ladle for different fuels: (a) natural gas, (b) converter gas, (c) coke oven gas

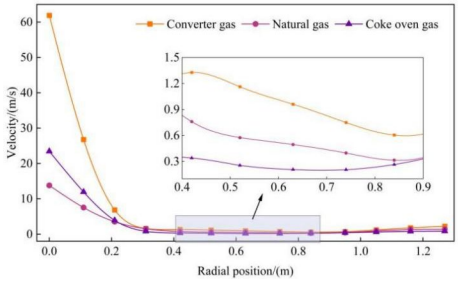



Fig. 4. Velocity distribution at $H$=2 m: (a) natural gas, (b) converter gas, (c) coke oven gas

## 3.2. Effect of fuel type on flame morphology

Figure 5 presents the evolution characteristics of flame width during the baking process with three fuels at the cross-section of $H$=1.3 m. It can be seen that the width of the high-temperature flame zone shows a continuous expansion trend with the extension of baking time. Throughout the entire preheating period, natural gas and converter gas maintain a complete and rounded flame morphology, while the flame of coke oven gas exhibits obvious irregularities.

At the cross-section of $H$=1.3 m, the flames of the three types of gas all expand gradually as baking time increases, yet their expansion rates differ significantly. For natural gas, the flame diameter increases from 0.45 m at 10 min to 0.55 m at 20 min. The flame diameter rises by approximately 0.05 m per 5 minutes of baking time, with a steady expansion rate. The flame diameter of converter gas increases from 0.35 m at the initial stage (10 min) to 0.45 m at 20 min. In the early preheating stage (10-15 min), its expansion rate is about 0.05 m/5min, basically equivalent to that of natural gas; in the late preheating stage (15-20 min), the expansion rate decreases to 0.025 m/5min, showing a distinct deceleration feature. Coke oven gas possesses the overall fastest flame expansion rate, with the flame diameter growing from 0.30 m at 10 min to 0.45 m at 20 min. Its early-stage (10-15 min) expansion rate reaches 0.10 m/5min, which is remarkably higher than those of natural gas and converter gas. In the later stage (15-20 min), the expansion rate drops sharply to 0.025 m/5min, consistent with the late expansion rate of converter gas.

In terms of temperature field distribution, the temperature field of natural gas follows a distribution pattern of high temperature in the center and gradual temperature gradient attenuation in the surrounding area. The high-temperature zone features a stable morphology and uniform temperature transition at the periphery. This is mainly attributed to the high calorific value and excellent flame rigidity of natural gas, which realize uniform and rapid preheating of scrap in the ladle. In the initial stage of converter gas combustion, the proportion of the low-temperature zone is relatively high, and the high-temperature zone expands gradually with baking time. Nevertheless, a prominent temperature gradient always exists between the central high-temperature area and the edge region, which is closely associated with its low calorific value and poor combustion stability. By contrast, coke oven gas shows the most irregular temperature field morphology, with scattered low-temperature zones and a time-dependent variable high-temperature zone. It delivers a slow heating rate and poor temperature field stability, primarily resulting from its low calorific value and the difficulty in forming a stable heat flow during combustion.

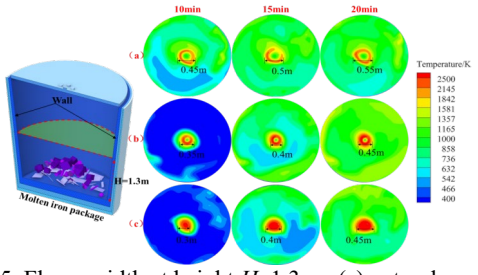



Fig. 5. Flame width at height $H$=1.3 m: (a) natural gas, (b) converter gas, (c) coke oven gas

Figure 6 reveals the evolution law of flame morphology at different moments during scrap preheating with different fuels in the ladle. It is evident that fuel type exerts a significant regulatory effect on flame structure. Under the preheating condition with natural gas (Fig. 6a), the main flame remains straight and the overall structure is stable and uniform with the extension of heating time, and the bottom expands outward in a regular fan shape. This characteristic is mainly attributed to methane-dominated components of natural gas, which enables stable and controllable combustion. With high flame temperature and strong flame rigidity, natural gas combustion forms a regular and symmetrical flame morphology.

Due to the high jet velocity of converter gas, its flame is slender (Fig. 6b) with distinct dendritic bifurcation at the bottom. Affected by the complex combustion characteristics of multi-component gases such as CO and $H_2$, the flame presents poor stability. Meanwhile, the uneven heat flow scattering caused by stacked scrap at the bottom further intensifies the airflow disturbance inside the ladle.

The flame of coke oven gas shows a continuous fragmented distribution (Fig. 6c). At the initial combustion stage, the flame is relatively slender, and obvious low-temperature zones persist at the bottom. This indicates its low flame temperature and slow heating rate, making it difficult to rapidly raise the temperature of scrap in the ladle within a short period. The above phenomenon is mainly caused by the abundant multi-hydrocarbon components including $H_2$, $CH_4$ and $C_mH_n$ in coke oven gas as well as its low overall calorific value. Such properties restrict continuous flame combustion and inhibit the formation of stable and regular heat flow structures.

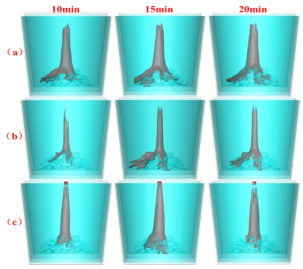



Fig. 6. Flame shape of the three gases at different heating times: (a) natural gas, (b) converter gas, (c) coke oven gas

## 3.3 Effect of fuel type on temperature field inside the ladle and scrap temperature rise

Figure 7 comparatively analyzes the temperature field distribution of the three gases at different moments during the ladle preheating process. The results show that, as the baking time increases from 10 min to 20 min, all three working conditions present common characteristics, including an overall temperature rise inside the ladle, continuous expansion of the high-temperature zone, gradual shrinkage of the low-temperature zone, and reduction of thermal stagnant dead zones. The maximum temperature in the ladle reaches 2800 K under the natural gas preheating condition, followed by converter gas at approximately 2400 K, while the maximum temperature of coke oven gas is only 1100 K, which is significantly lower than the former two fuels.

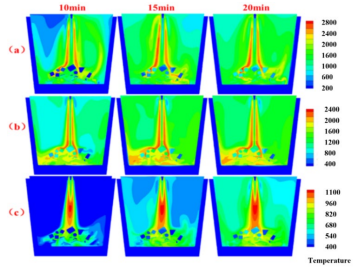



Fig. 7. Temperature distribution inside the ladle for different fuels: (a) natural gas, (b) converter gas, (c) coke oven gas

Comparing the temperature field distribution at 10 min, converter gas exhibits the fastest heating rate and the best temperature uniformity in the ladle at the end of preheating. It indicates that under the condition of similar calorific values, the preheating performance of converter gas is superior to that of natural gas and coke oven gas. During the preheating process of natural gas and coke oven gas, the temperature on the right side of the ladle is obviously higher than that on the left side due to the accumulation and distribution of scrap at the bottom. This phenomenon reveals that the increase in gas flow velocity can expand the vortex range of the flow field and strengthen turbulent disturbance, thereby enhancing heat diffusion and transport, continuously expanding the high-temperature area and steadily raising the overall temperature level in the ladle. It reflects the driving effect of flow field structure on heat transfer. Meanwhile, the formation and evolution of the high-temperature zone also exert a feedback effect on flow field characteristics. Adjusting the gas flow rate can change the circulation intensity of the internal flow field, so as to realize effective regulation and control of the temperature field distribution.

Figure 8 presents the three-dimensional temperature distribution characteristics of scrap piles under natural gas, converter gas and coke oven gas at the preheating durations of 10 min, 15 min and 20 min. As the preheating time increased from 10 min to 20 min, the scrap temperature under all working conditions showed a continuous upward trend. At the preheating time of 10 min, the scrap pile was mainly covered by the low-temperature zone of 300-480 K, and only a small temperature rise occurred in the local upper scrap, indicating that the heat was mainly concentrated on the surface layer of scrap at the initial preheating stage. At 15 min, the internal temperature gradient of the scrap pile increased significantly, the proportion of the medium-temperature region of 540-720 K increased obviously, and heat began to transfer from the surface to the interior of the scrap pile. When the preheating proceeded to 20 min, the coverage of the medium and high-temperature zone of 720-780 K was further expanded under all conditions, and the overall temperature uniformity of the scrap pile was improved, which reflected the accumulation and strengthening effect of heat transfer in the later preheating stage [20].

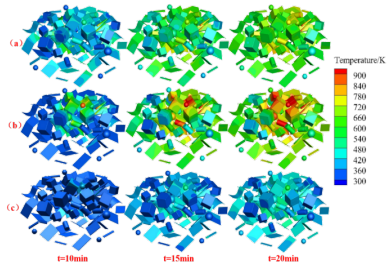



Fig. 8. Preheating temperature of scrap at different times: (a) natural gas, (b) converter gas, (c) coke oven gas

Different gas types impose remarkably distinct effects on scrap preheating performance. Under the natural gas condition (Fig. 8a), the temperature rise of scrap was relatively gentle, which gradually transited from the low-temperature zone to the medium-temperature zone of 540-720 K within 10-20 min. The temperature field exhibited favorable uniformity, while the proportion of the overall high-temperature zone was relatively low, which was closely related to its moderate combustion heat release intensity. The heating performance of converter gas (Fig. 8b) was more prominent. Local high-temperature zones above 720 K appeared after 15 min, and the medium and high-temperature zones became dominant at 20 min, demonstrating that the combustion and heat release characteristics of converter gas were more conducive to the efficient internal heat transfer inside the scrap pile. By contrast, the temperature rise under coke oven gas condition (Fig. 8c) showed an obvious hysteresis. Even after 20 min of preheating, the scrap pile was still dominated by the low-temperature zone below 480 K. This is mainly attributed to its low calorific value and low combustion efficiency, which cannot supply sufficient heat for rapid temperature rise of scrap.

The above results reveal that the combustion characteristics of gas directly determine the distribution and evolution of the

temperature field during scrap preheating. Converter gas achieved the highest preheating peak temperature of 782 K, which was increased by 12.52% and 90.27% compared with natural gas and coke oven gas, respectively. Despite its relatively low calorific value, the high-velocity jet leads to concentrated combustion heat release, and the intense turbulent disturbance greatly improves the heat transfer efficiency inside the ladle. Natural gas ranked second with a peak preheating temperature of 695 K, and its stable and uniform heat release behavior facilitated heat transfer and temperature homogenization in the gaps among scrap materials. Coke oven gas had the lowest preheating temperature of 411 K. Restricted by its low calorific value, the insufficient heat supply failed to realize effective and rapid heating of scrap.

The results further indicate that the upper scrap has a faster temperature rise due to direct contact with high-temperature flame and flue gas, while the bottom scrap is affected by stacking shielding and heat transfer attenuation, presenting a relatively slow heating rate.

Figure 9 illustrates the variation of the average surface temperature of scrap with fuel flow rate under different fuel conditions. As shown in Fig. 9a, under the condition of identical calorific value input, the average surface temperature of scrap preheated by natural gas, converter gas and coke oven gas is approximately 799 K, 943 K and 468 K, respectively. This indicates that fuel type acts as a critical factor dominating the temperature level of scrap preheating. The above temperature differences mainly stem from the discrepancies in calorific value, combustion reaction rate and radiation characteristics of combustion products among different fuels. At the same heat input, the required volumetric flow rate of converter gas is significantly higher than that of natural gas and coke oven gas. Its high-velocity flow behavior strengthens the turbulent mixing and heat transfer process in the ladle, thereby achieving a superior heating performance.

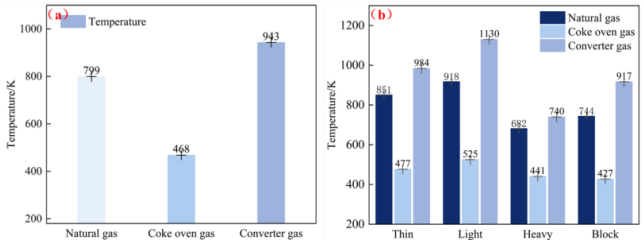



Fig. 9. Average surface temperature of scrap under different fuel types after 30 min preheating

Further analysis on the preheating characteristics of different types of scrap (Fig. 9b) shows that the preheating temperatures of light scrap under the three fuels are 918 K, 525 K and 1130 K, while those of thin and light scrap are 851 K, 477 K and 984 K, respectively. It can be observed that both light scrap and thin-light scrap present a higher preheating temperature than the overall average level of scrap under all fuel conditions. This is closely associated with their large specific surface area and low heat capacity, enabling them to absorb heat rapidly and achieve a fast temperature rise. In contrast, the maximum preheating temperatures of medium-heavy scrap and bundled scrap are only about 740 K and 917 K under various fuel atmospheres, with a limited overall temperature increment. Such a result is primarily attributed to their large bulk density, compact structure and complex shape, which hinder rapid heat transfer to the inner core region of scrap within a short time.

Based on the above preheating laws of scrap, the following conclusion can be drawn: to avoid overheating or melting of thin-light scrap during preheating and maximize energy utilization efficiency, natural gas is more appropriate for preheating. Its moderate heat release and uniform temperature field distribution can effectively restrain local overheating. In contrast, for heavy scrap and bundled scrap with poor thermal conduction and difficult deep heating, high heat flux density fuels such as converter gas are recommended to ensure that the core temperature of scrap meets the requirements of metallurgical processes.

Figure 10 compares the flame morphology and temperature distribution characteristics of natural gas, converter gas and coke oven gas at different cross-sectional heights inside the ladle. From the radial cross-sectional perspective, the flame distribution of the three gases follows an evolution trend of "concentration–diffusion" as the height decreases. At the height of $H$=1.07 m (Fig. 10a), the flame is dominated by a concentrated high-temperature core zone with a regular morphology and a large temperature gradient, reflecting the direct impact of flame jet and the rigid heat transfer characteristics. At $H$=0.76 m (Fig. 10b), the radial width of the flame expands obviously and the coverage of the high-temperature zone increases, accompanied by a gentle temperature gradient. This phenomenon is caused by the stacking obstruction of the scrap pile and the heat transfer effect, which jointly change the flame propagation pattern. At $H$=0.45 m (Fig. 10c), the flame structure is further dispersed and the overall temperature declines, indicating an obvious energy attenuation effect during heat transfer toward the ladle bottom.

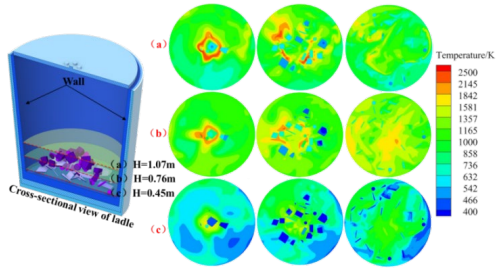



Fig. 10. Flame width at different heights: (a) natural gas, (b) converter gas, (c) coke oven gas

In terms of gas type comparison, significant differences exist in flame performance and temperature distribution of various fuels at each cross-section. For natural gas, the flame morphology remains regular at all heights. A concentrated high-temperature core is formed at $H$=1.07 m, and the temperature uniformity is greatly improved at $H$=0.45 m while maintaining a relatively high overall temperature, which demonstrates its excellent combustion stability and uniform heat flow diffusion capacity. Converter gas presents the most prominent flame diffusion at $H$=0.76 m, and its high-temperature coverage is distinctly larger than those of natural gas and coke oven gas, which is consistent with its high combustion heat release intensity, intense turbulent disturbance and superior heat flow diffusion performance. By contrast, coke oven gas is characterized by narrow flame width, weak high-temperature intensity and low overall temperature at all cross-sections.

Restricted by low calorific value and poor combustion efficiency, it is difficult to form an obvious high-temperature core even at $H$=1.07 m, resulting in much lower heat transfer efficiency than the other two gases.

Figure 11 compares the temporal variation of scrap temperature during preheating with different fuel gases. The results indicate that the surface temperature of scrap continuously increases with preheating time under all three gas conditions. In the early stage of preheating, the temperature curve rises rapidly with small fluctuations; in the middle and late stage, the temperature rise slows down, and local slight fluctuations appear due to the unstable combustion of individual fuels.

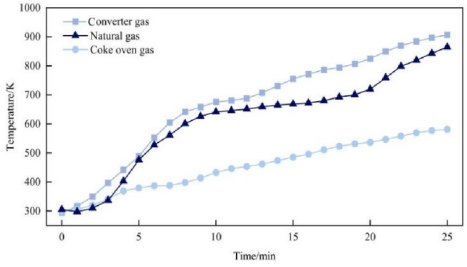



Fig. 11. Preheating temperature of scrap surface under different fuel types

Under the converter gas condition, the scrap surface temperature remains the highest throughout the entire preheating period, reaching nearly 900 K at 25 min. Under the same calorific input, converter gas possesses a higher volumetric flow rate and more concentrated combustion heat release. Meanwhile, its high jet velocity strengthens thermal radiation and convective heat transfer, which accelerates heat delivery to the scrap surface and achieves efficient temperature rise.

The temperature rise curve of scrap under natural gas is slightly lower than that of converter gas, with a terminal temperature of approximately 850 K. Natural gas maintains stable combustion and provides a sustained and uniform preheating environment for scrap. Coke oven gas exhibits the poorest preheating performance, with a final temperature of only about 600 K. Restricted by its complex components and low calorific value, coke oven gas produces low-temperature flue gas and a poorly uniform thermal field, resulting in low heat transfer efficiency and a severely limited heating capacity for scrap.

## 3.4. Analysis of preheating efficiency for different fuel types

Figure 12 presents the variation characteristics of gas utilization efficiency during scrap preheating with different fuels, which intuitively reflects the regulatory effect of fuel physical properties on energy utilization performance. At the end of preheating, the average surface temperature of scrap under natural gas, converter gas and coke oven gas conditions is 799 K, 943 K and 468 K, corresponding to gas utilization efficiencies of 5.9%, 11.2% and 2.4%, respectively.

It can be seen that converter gas achieves the highest preheating efficiency, followed by natural gas, while coke oven gas shows the lowest value with significant differences among the three fuels. This demonstrates that gas type exerts a decisive influence on the energy utilization efficiency of the preheating process. Benefiting from its high injection velocity, converter gas remarkably enhances convective heat transfer and internal heat transport inside the ladle, thereby obtaining the optimal energy utilization efficiency. Although natural gas has a high calorific value, the stacked structure of scrap hinders the sufficient heat transfer to the lower-layer scrap. A portion of thermal energy cannot be fully utilized, resulting in a lower efficiency than that of converter gas. Due to the low inherent calorific value and limited combustion efficiency of coke oven gas, its heat supply and heat transfer capacity are insufficient, which ultimately leads to the poorest energy utilization level.

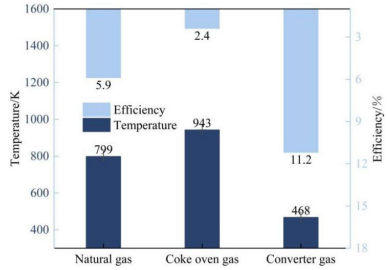



Fig. 12. Fuel utilization efficiency under different fuel types

# 4. Conclusion

In this study, a three-dimensional numerical model for scrap preheating with disordered stacking structures was established. The combustion, heat and mass transfer behaviors during scrap preheating using different fuel gases were investigated. Under the identical baking duration and heat input conditions, the preheating performance of three fuels was compared by means of numerical simulation. The effects of natural gas, coke oven gas and converter gas on the scrap preheating process were systematically revealed, and the main conclusions are summarized as follows:

1) The flame morphology, flow field structure and heat transfer intensity inside the ladle are closely dependent on fuel gas type. Under the same heat input, natural gas and converter gas present regular flame shapes and superior flame rigidity. The high flow velocity of converter gas leads to strong turbulent disturbance, while natural gas with high calorific value has low inlet flow rate and mild flow field. By contrast, coke oven gas exhibits fragmented flames and a disordered flow field due to its low calorific value, resulting in the poorest preheating stability.
2) Significant differences exist in the temperature rise performance and preheating efficiency of scrap for the three fuel gases. Within the same baking time, the average surface temperature of scrap follows the order: converter gas 782 K, natural gas 695 K, and coke oven gas 411 K. The corresponding preheating efficiencies are 11.2%, 5.9% and 2.4%, respectively. Restricted by its low calorific value, coke oven gas shows a far inferior overall preheating effect compared with the other two gases.

3) There is an optimal matching relationship between fuel gas categories and scrap types. With mild combustion characteristics and uniform temperature distribution, natural gas is suitable for preheating thin and light scrap to prevent overheating. Converter gas features high heat flux density and excellent thermal penetration capacity, which is more applicable for medium-heavy scrap and bundled scrap. The research conclusions can provide direct guidance for fuel selection in industrial production and low-carbon smelting with a high scrap ratio.

## Acknowledgments

The authors are grateful for the financial support by Innovation and Entrepreneurship Training Program for College Students and the Project of Liaoning Provincial Department of Science and Technology (2025-BSLH-189).

## References

[1] Cai, X.Y., Duan, H.J., Ding, D.H., Xu, A.J. & Zhang, L.F. (2024). Water modeling on fluid flow and mixing phenomena in a BOF steelmaking converter. *Journal of Iron and Steel Research International*. 31(3), 595-607. DOI: 10.1007/s42243-023-01072-7.

[2] Burkert, J. & Schwarze, R. (2025). Analysis of surface behavior and cavity oscillations in a liquid metal model experiment of the basic oxygen furnace process. *Steel Research International*. 96(5), 2300184, 1-9. DOI: 10.1002/srin.202300184.

[3] Quiyoom, A., Ajmani, S.K. & Buwa, V.V. (2018). Optimization of bottom tuyere configuration for basic oxygen furnace steelmaking through experiments and CFD simulations. *Chemical Engineering Journal*. 346(1), 127-142. DOI: 10.1016/j.cej.2018.03.122.

[4] Tago, Y. & Higuchi, Y. (2003). Fluid flow analysis of jets from nozzles in top blown process. *ISIJ international*. 43(2), 209-215. DOI: 10.2355/isijinternational.43.209.

[5] Alam, M., Naser, J. & Brooks, G. (2010). Computational fluid dynamics simulation of supersonic oxygen jet behavior at steelmaking temperature. *Metallurgical & Materials Transactions B*. 41(3), 636-645. DOI: 10.1007/s11663-010-9341-0.

[6] Giannadakis, A., Naxakis, A., Romeos, A., Perrakis, K. & Panidis, T. (2019). An experimental study on a coaxial flow with inner swirl: Vortex evolution and flow field mixing attributes. *Aerospace Science and Technology*. 94, 105373, 1-16. DOI: 10.1016/j.ast.2019.105373.

[7] Jiang, P., & He, X. (2020). Experimental investigation of flow field characteristics in a mixed-flow trapped vortex combustor. *Aerospace Science and Technology*. 96, 105533, 1-11. https://doi.org/10.1016/j.ast.2019.105533.

[8] Hu, X., Zhang, J., Yu, Z., Liu, Z., Guo, J. & Xu, C. (2024). Numerical study of the combustion process in the vertical heating flue of air staging coke oven. *Processes*. 12(10), 2294, 1-19. DOI: 10.3390/pr12102294.

[9] Fan, W., Li, Y., Guo, Q., Chen, C. & Wang, Y. (2017). Coalnitrogen release and NOx evolution in the oxidant-staged combustion of coal. *Energy*. 125, 417-426. DOI: 10.1016/j.energy.2017.02.130.

[10] Vodička, M., Hrdlička, J. & Skopec, P. (2021). Experimental study of the NOx reduction through the staged oxygen supply in the oxy-fuel combustion in a 30 kWth bubbling fluidized bed. *Fuel*. 286, 119343, 1-9. DOI: 10.1016/j.fuel.2020.119343.

[11] Zhang, H., Zhou, P. & Yuan, F. (2021). Effects of ladle lid or online preheating on heat preservation of ladle linings and temperature drop of molten steel. *Energy*. 214, 118896, 1-11. DOI: 10.1016/j.energy.2020.118896.

[12] Poraj, J., Gamrat, S., Bodys, J., Smolka, J. & Adamczyk, W. (2016). Numerical study of air staging in a coke oven heating system. *Clean Technologies and Environmental Policy*. 18(6), 1815-1825. DOI: 10.1007/s10098-016-1234-8.

[13] Campos, M.G.G., Dos Santos, M.F., Moreira, M.H., Angélico, R.A., Sako, E.Y. & Pandolfelli, V.C. (2020). Holistic view of the insulating layer on the thermal efficiency of a steel ladle lining. *International Journal of Ceramic Engineering & Science*. 2(3), 113-129. DOI: 10.1002/ces2.10043.

[14] Li, Z., Yi, Q., Zhang, Y., Zhou, H., Zhao, Y., Huang, Y. & Hao, Y. (2020). Numerical study and design strategy for a low emission coke oven system using oxy-fuel combustion of coke oven gas. *Journal of Cleaner Production*. 252, 119656, 1-15. DOI: 10.1016/j.jclepro.2019.119656.

[15] Li, M.M., Li, L., Li, Q. & Zou, Z.S. (2018). Modeling of mixing behavior in a combined blowing steelmaking. *JOM: The Journal of the Minerals, Metals & Materials Society*. 70(10), 2051-2058. https://doi.org/10.1007/s11837-018-2889-x.

[16] Liu, Z., Cheng, S. & Peng, J. (2024). Simulation of fluid flow in the top–bottom combined blowing converter. *Metals*. 14(1), 56, 1-21. DOI: 10.3390/met14010056.

[17] Lv, M., Zhu, R., Guo, Y.G. & Wang, Y.W. (2013). Simulation of flow fluid in the BOF steelmaking process. *Metallurgical & Materials Transactions B*. 44(6), 1560-1571. DOI: 10.1007/s11663-013-9935-4.

[18] Zhou, Z., Han, X., Wang, X., Yu, J. & Shan, S. (2023). New coefficients of the weighted-sum-of-gray-gases model for gas radiation characteristics of hydrogen/natural gas blends combustion. *International Communications in Heat and Mass Transfer*. 149, 107090, 1-10. DOI: 10.1016/j.icheatmasstransfer.2023.107090.

[19] Park, Y.K. & Kim, B.S. (2023). Catalytic removal of nitrogen oxides (NO, $NO_2$, $N_2O$) from ammonia-fueled combustion exhaust: A review of applicable technologies. *Chemical Engineering Journal*. 461, 141958, 1-13. DOI: 10.1016/j.cej.2023.141958.

[20] Calvo, W.A., Dignani, M.L., Galliano, P.G., Brandaleze, E. & Martínez, A.G.T. (2022). Basic slag corrosion of alumina–magnesia–carbon refractory bricks containing Al and Si antioxidants. *International Journal of Applied Ceramic Technology*. 19(4), 2331-2343. DOI: 10.1111/ijac.14017.